

# Equator and High-Latitude Ionosphere-to-Magnetosphere Research

**B. W. Reinisch  
G. S. Sales  
V. Paznukhov  
I. A. Galkin**

**Q. Zong  
G. Khmyrov  
V. Galushko  
D. F. Altadill**

**University of Massachusetts Lowell  
Center for Atmospheric Research  
600 Suffolk Street  
Lowell, MA 01854**

**4 December 2010**

**Scientific Report No. 4**

**Approved for public release. Distribution unlimited.**



**AIR FORCE RESEARCH LABORATORY  
Space Vehicles Directorate  
29 Randolph Road  
AIR FORCE MATERIEL COMMAND  
HANSCOM AFB, MA 01731-3010**

---



# REPORT DOCUMENTATION PAGE

*Form Approved*  
*OMB No. 0704-0188*

Public reporting burden for this collection of information is estimated to average 1 hour per response, including the time for reviewing instructions, searching existing data sources, gathering and maintaining the data needed, and completing and reviewing this collection of information. Send comments regarding this burden estimate or any other aspect of this collection of information, including suggestions for reducing this burden to Department of Defense, Washington Headquarters Services, Directorate for Information Operations and Reports (0704-0188), 1215 Jefferson Davis Highway, Suite 1204, Arlington, VA 22202-4302. Respondents should be aware that notwithstanding any other provision of law, no person shall be subject to any penalty for failing to comply with a collection of information if it does not display a currently valid OMB control number. **PLEASE DO NOT RETURN YOUR FORM TO THE ABOVE ADDRESS.**

<b>1. REPORT DATE (DD-MM-YYYY)</b> 04-12-2010			<b>2. REPORT TYPE</b> Scientific Report #4			<b>3. DATES COVERED (From - To)</b> 26 Aug 2009 – 25 Aug 2010		
<b>4. TITLE AND SUBTITLE</b> Equator and High-Latitude Ionosphere-to-Magnetosphere Research						<b>5a. CONTRACT NUMBER</b> FA8718-06-C-0072		
						<b>5b. GRANT NUMBER</b>		
						<b>5c. PROGRAM ELEMENT NUMBER</b> 62601F		
<b>6. AUTHOR(S)</b> B. W. Reinisch, G. Sales, V. Paznukhov, I. Galkin, Q. Zong, G. Khmyrov, V. Galushko, D. Altadill						<b>5d. PROJECT NUMBER</b> 4827		
						<b>5e. TASK NUMBER</b> HR		
						<b>5f. WORK UNIT NUMBER</b> A1		
<b>7. PERFORMING ORGANIZATION NAME(S) AND ADDRESS(ES) AND ADDRESS(ES)</b> University of Massachusetts Lowell Center for Atmospheric Research 600 Suffolk St. Lowell MA 01854						<b>8. PERFORMING ORGANIZATION REPORT NUMBER</b>		
<b>9. SPONSORING / MONITORING AGENCY NAME(S) AND ADDRESS(ES)</b>  Air Force Research Laboratory 29 Randolph Road Hanscom AFB MA 01731-3010						<b>10. SPONSOR/MONITOR'S ACRONYM(S)</b> AFRL/RVBXI		
						<b>11. SPONSOR/MONITOR'S REPORT NUMBER(S)</b> AFRL-RV-HA-TR-2010-1138		
<b>12. DISTRIBUTION / AVAILABILITY STATEMENT</b> Approved for public release: distribution unlimited.								
<b>13. SUPPLEMENTARY NOTES</b>								
<b>14. ABSTRACT</b> Significant research effort has been directed at global ionospheric specification using the UML-operated Global Ionospheric Radio Observatory (GIRO). In 2010, GIRO continued acquisition and dissemination of both real-time and retrospective knowledge of electron density profile (EDP) in the ionosphere from 64 digisonde locations around the world. Highly accurate, manually validated EDP records from GIRO were used to calibrate DMSP F18 UV sensors and quantify errors introduced by the horizontal smear of COSMIC radio occultations. Comparative analysis of the profile inversion algorithms against incoherent scatter radar measurements has identified a deficiency of the POLAN technique used in QualScan software involved in EDP uncertainty analysis for AFWA. The utility of the high-resolution and high cadence Doppler skymaps in characterizing plasma velocity profile in the heated region above HAARP has been clearly established. Specification of D region absorption from Digisonde measurements has been proven to be highly sensitive to so as to detect and model M-class flare events.								
<b>15. SUBJECT TERMS</b> GIRO, Digisonde, Electron density profile, Ground truth, Cal/Val, Doppler skymap, HAARP, Plasma velocity profile, Ionogram autoscaling, D region absorption, Real-time data assimilation.								
<b>16. SECURITY CLASSIFICATION OF:</b>						<b>17. LIMITATION OF ABSTRACT</b>  UNL	<b>18. NUMBER OF PAGES</b>	<b>19a. NAME OF RESPONSIBLE PERSON</b> Kenneth Walker
<b>a. REPORT</b> UNCL	<b>b. ABSTRACT</b> UNCL	<b>c. THIS PAGE</b> UNCL	<b>19b. TELEPHONE NUMBER (include area code)</b>					



## Contents

<b>1 OVERVIEW</b> .....	1
<b>2 GLOBAL IONOSPHERIC RADIO OBSERVATORY</b> .....	2
2.1 Introduction .....	2
2.2 Analysis of GIRO data uncertainty .....	2
<b>3 HAARP INVESTIGATIONS</b> .....	5
3.1 Introduction .....	5
3.2 February 2010 BRIOCHE Campaign .....	6
3.3 Progress in Analysis of November 2009 Campaign .....	8
3.4 Upgrading the HAARP Digisonde Facility .....	9
3.5 Supporting HAARP experiments using the HAARP/Gakona Digisonde ..	11
3.6 Future Effort .....	11
<b>4 RESEARCH INTO SELF-SCATTERING EFFECTS</b> .....	12
4.1 Introduction .....	12
4.2 February 2010 HAARP Scattering Campaign .....	12
4.3 March 2010 EISCAT Campaign .....	12
<b>5. D-REGION ABSORPTION USING DIGISONDE DATA</b> .....	13
5.1 Introduction .....	13
5.2 Median D-region profile .....	13
5.3 Flare profile .....	16
5.4 Recommendations .....	16
<b>6. STUDY OF THE IONOSPHERIC RESPONSE TO STRONG GEOMAGNETIC STORMS</b> .....	17
6.1 Progress .....	17
<b>7 COMPARING COSMIC/FORMOSAT EDP WITH DIGISONDE PROFILES</b> .....	20
7.1 Introduction .....	20
<b>PUBLICATIONS</b> .....	24
<b>REFERENCES</b> .....	26



## Figures

1. Map of digisondes contributing data to GIRO. Red stars identify online digisondes providing data to GIRO in near-real-time, blue stars denote locations whose retrospective data collections are held in the GIRO archives, and green stars correspond to future installations planned by AFWA. 3
2. Profile calculation by NHPC and POLAN algorithms used in the QualScan analysis to derive the EDP uncertainty for GAIM assimilation. This example of a nighttime profile at low solar activity shows large height discrepancies of up to 50 km. 4
3. NHPC and POLAN profiles compared to radar data at Arecibo (high solar activity). NHPC (red curve) uses a night-time valley model, whereas POLAN uses a model for start height of ionosphere at 0.5 MHz. 5
4. Doppler sky maps from the HAARP digisonde during the heating experiment 02/04/10: (top) 2 min prior and (bottom) 9 min into the HF-heating. 7
5. The Doppler shift for a given probing frequency measured at different altitudes between 335 and 370 km. 8
6. Simultaneous measurements made on November 16, 2009 by the HAARP DPS-4D system and the collocated all-sky camera. The skymap echoes in these maps come from the height of the additional layer observed in the ionogram. The HF and optical images are remarkably similar. 9
7. Median daytime absorption (dB) for Boulder, CO digisonde as a function of sounding frequency. Also shown is the upper 2-sigma curve for the routine measurements. The figure also shows the enhanced absorption following the two M-class flares on 22 and 23 August 2005. 14
8. Absorption as a function of frequency for the August noontime data (solid curves). Black: digisonde absorption. Red: Absorption derived from the electron density profile. Flare absorptions are shown as dashed curves. 15
9. Derived electron density profiles that best fits the measured absorption data; black – median noontime profile, red – flare profile. 16
10. Geomagnetic storm of 15 May 2005 as observed with the DPS-4 at Kwajalein. The effect on the ionospheric layer height is clearly seen (lower panel). The effect on the electron density (middle panel) is significantly weaker. 19
11. RO measurement made in the vicinity of Kwajalein station on February 17, 2007. The blue symbols show radial projections of tangent points at which electron density is measured. The red star indicates the Kwajalein digisonde location. Horizontal smear parameter represents the length of the projection. 20

12. RO measurement error as a function of occultation smear calculated for Tromso location. Majority of measurements have horizontal smears smaller than 1000 km. 21
13. RO measurement error as a function of occultation smear calculated for Tromso. The data are binned according to the smear value, and the median error is calculated for each data bin. The overall trend indicates larger errors for greater horizontal smears. 22
14. RO measurement error as a function of occultation smear calculated for Ebro. The data are binned according to the smear value, and median error is calculated for each data bin. The overall trend shows larger error for greater horizontal smears, as expected. 22
15. RO measurement error as a function of occultation smear calculated for Kwajalein. Note different scale of the y-axis with respect to Figure 11. The data are binned according to the smear value, and median error is calculated for each data bin. 23

## Tables

1.	Prioritized Software Capabilities Guidance List	10
2.	UMLCAR-supported experiments at HAARP	11
3.	Major storms of 1997-2006	18

## ACRONYMS

AF	Air Force	
AFRL	Air Force Research Laboratory	
AFWA	Air Force Weather Agency	
ARTIST	Automatic Real-Time Ionogram Scaler with True height	
BRIOCHE	Basic Research on Ionospheric Characteristics and Effects	
CHAMP	CHAllenging Minisatellite Payload	
C/NOFS	Communications/Navigation Outage Forecasting System	
COSMIC	Constellation Observing System for Meteorology, Ionosphere &	Climate
DCART	Digisonde Commanding and Acquisition Remote Terminal	
DEMETER	Detection of Electro-Magnetic Emissions Transmitted from Earthquake Regions	
DMSP	Defense Meteorological Satellite Program	
DPS	Digisonde Portable Sounder	
EDP	Electron Density Profile	
EISCAT	European Incoherent Scatter Scientific Association	
GAIM	Global Assimilation of Ionospheric Measurements	
GIRO	Global Ionospheric Radio Observatory	
HAARP	High frequency Active Auroral Research Program	
HF	High Frequency	
IRA	Institute of Radio Astronomy	
MZ	Magnetic Zenith	
NHPC	N(h) inversion for Personal Computer	
POLAN	Polynomial Analysis program	
RO	Radio Occultation	
UMLCAR	University of Massachusetts Lowell Center for Atmospheric Research	
USU	Utah State University	

## 1 OVERVIEW

The efforts described in this report support the ionospheric specification program of the Air Force Research Laboratory (AFRL). The University of Massachusetts Lowell Center for Atmospheric Research (UMLCAR) has taken an approach that addresses the specification of ionospheric parameters on a global scale; a goal that is particularly facilitated using the UMLCAR-operated Global Ionospheric Radio Observatory (GIRO) [Reinisch and Galkin, 2010]. The GIRO provides both real-time and retrospective knowledge of the ionospheric plasma distribution at 65 worldwide locations of the Digisonde ionospheric sounding system [Reinisch *et al.*, 2004]. Such global ionospheric specification and associated global assimilative ionospheric modeling is a major part of space weather forecasting and global communications progress. It is also instrumental to verification and validation of other sensor systems for ionospheric specification, in which GIRO measurements are the “truth” against which their performance is compared. Our support for these goals is presented here.

Ground-based data from ionosondes have been used in this program to develop the basis for a global empirical ionosphere electron density ( $N_e$ ) model that extends from the E region to the plasmapause. It is generally accepted that ionosphere models need real time drivers, the most important one being the F2 layer peak parameters. Our research is aimed at establishing the accuracy of these real time drivers derived from the GIRO network (Section 2). Using the GIRO data holdings, extensive comparisons are made with other electron density profiling techniques to provide a ground truth for these measurements (Sections 7 and 8). Some of this work focuses on the equatorial ionosphere where incoherent scatter radar data can be used to validate the ionosonde  $N_e$  profiles and the plasma drifts measured by the collocated ionosonde, providing direct support for the AF C/NOFS mission (Section 6).

High latitude research has concentrated on self-scatter propagation studies over the polar cap using the HAARP transmitter (heater) and suitably located digisondes for reception at several stations (Sections 3 and 4). Irregularities generated by the high power heating are the source of self-scattering of the same heater signal, and the propagation of these signals are investigated by these experiments. Multiple receiving sites at mid latitude and in Antarctica reveal the azimuthal characteristics of this scattering as well as the existence of ducted modes.

Long distance radio communication is often limited by excessive D region absorption and real time drivers are required that can predict propagation outages. The measured amplitudes for vertical HF sounding are a reliable and sensitive measure of the D region absorption that can be made available from any digisonde station. Measurement of the absorption index will be one result of our research that can ultimately become part of a propagation forecast (Section 5).

Ionospheric disturbances, especially during magnetic storms and substorms, have detrimental effects on DoD communication systems. Precision group height has been implemented as an enhanced capability using digital sounders where two closely-spaced frequencies are used to obtain accurate virtual height data. This technique reveals changes in the E layer of the ionosphere, related to traveling ionospheric disturbances and geomagnetic activity (Section 6).

## 2 GLOBAL IONOSPHERIC RADIO OBSERVATORY

### 2.1 Introduction

Accurate global modeling of Earth's ionosphere requires data from around the globe and for a long time the data coverage has been inadequate. A quiet revolution in sensor network technologies started brewing in the late 1990s with the advent of low-cost information technology solutions that permitted researchers and engineers to acquire, archive, and access their sensor data without time or distance barriers. The quiet revolution has significantly impacted the network of Digisonde ionospheric sounders installed at 80+ locations in the world, gradually evolving their generally independent subsistence into a Global Ionospheric Radio Observatory (GIRO) portal, <http://giro.uml.edu>. The GIRO holds 30+ million records of ionospheric measurements collected at 64 locations, including 42 real time feeds (see Figure 1).

### 2.2 Analysis of GIRO data uncertainty

Analysis of the ARTIST-derived electron density profile (EDP) uncertainty is a cooperative effort with AFRL/Boston College to study effects of assimilating GIRO data in USU GAIM [McNamara, 2008]. QualScan processing [McNamara, 2006] was used in the study to obtain the ionogram-derived EDP uncertainties. The QualScan's concept of operations is to compare profiles derived from the same ARTIST trace using two independent techniques, (a) "N(h) inversion for Personal Computer" (NHPC) [Huang and Reinisch, 1982, 1996] and (b) "Polynomial Analysis" (POLAN) [Titheridge, 1985, 1988]. Comparative analysis of the NHPC versus POLAN techniques can be found in [Reinisch *et al.*, 1988]. QualScan reports one-half differences between two calculated profiles for each height as the point-by-point error bars of the EDP. While analysis of the obtained QualScan results is out of the scope of this report, we contrasted ARTIST-5 and QualScan techniques for evaluating the EDP uncertainty.

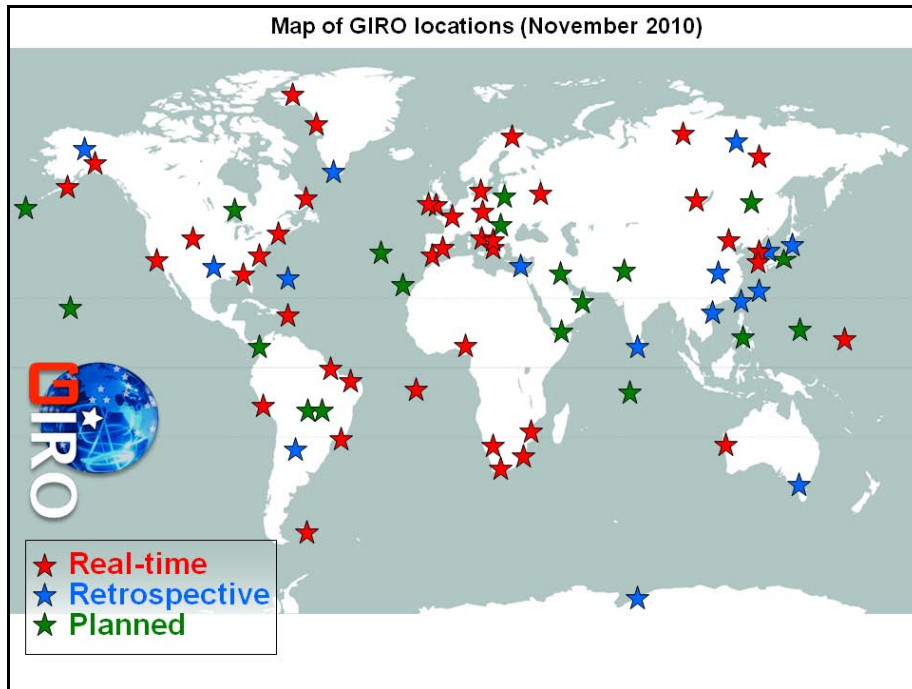


Figure 1. Map of digisondes contributing data to GIRO. Red stars identify online digisondes providing data to GIRO in near-real-time, blue stars denote locations whose retrospective data collections are held in the GIRO archives, and green stars correspond to future installations planned by AFWA.

In order to replicate the QualScan principles of per-point comparison of the NHPC and POLAN profiles, ARTIST-5 software was modified to spawn POLAN and read its results so that uncertainty of the profile inversion can be calculated and added to the uncertainties of the ARTIST autoscaling. Early testing showed large discrepancies of POLAN and NHPC results during nighttime periods and low foF2 critical frequencies (i.e., low solar activity). Figure 2 exemplifies conducted EDP comparisons for one digisonde measurement taken at Madimbo, South Africa, on November 1, 2008, 00:30 UT.

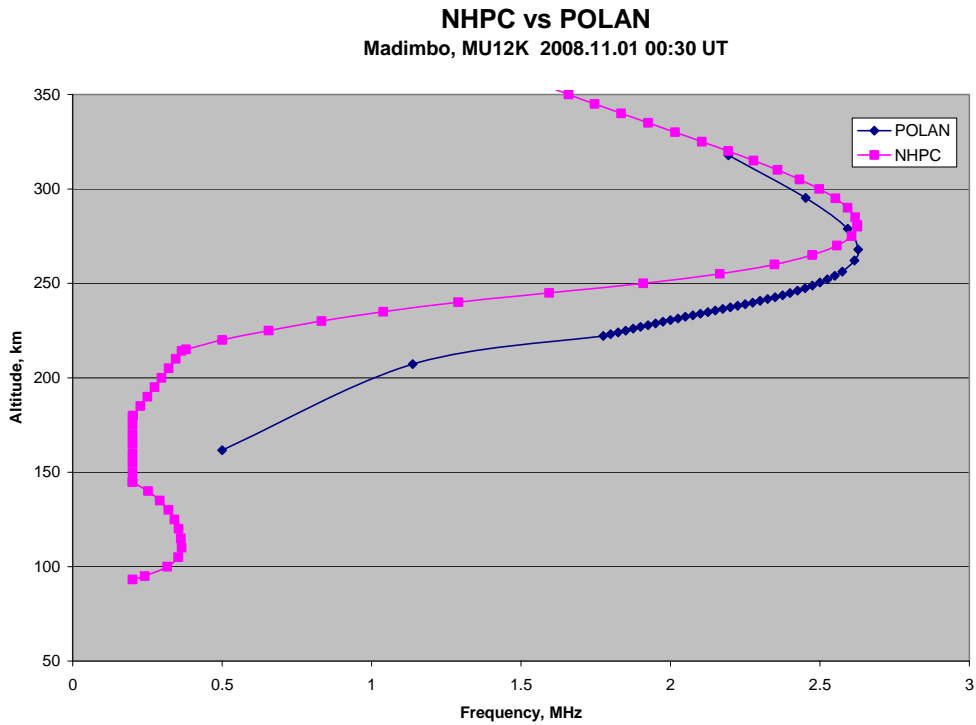


Figure 2. Profile calculation by NHPC and POLAN algorithms used in the QualScan analysis to derive the EDP uncertainty for GAIM assimilation. This example of a nighttime profile at low solar activity shows large height discrepancies of up to 50 km.

A more detailed analysis of EDP provided by NHPC and POLAN versus profiles measured by incoherent scatter radars in Millstone Hill and Arecibo has been conducted. Figure 3 presents a sample comparison of NHPC and POLAN profiles to the Arecibo incoherent scatter radar profile.

Similar NHPC vs. POLAN differences are seen in Figure 2 and 3, though discrepancies in April 2000 are smaller during this high solar activity period. NHPC (red curve) uses a night-time valley model [Chen *et al.*, 1994], whereas POLAN uses a model for the start height of the F layer at 0.5 MHz [Titheridge, 1988] and no valley.

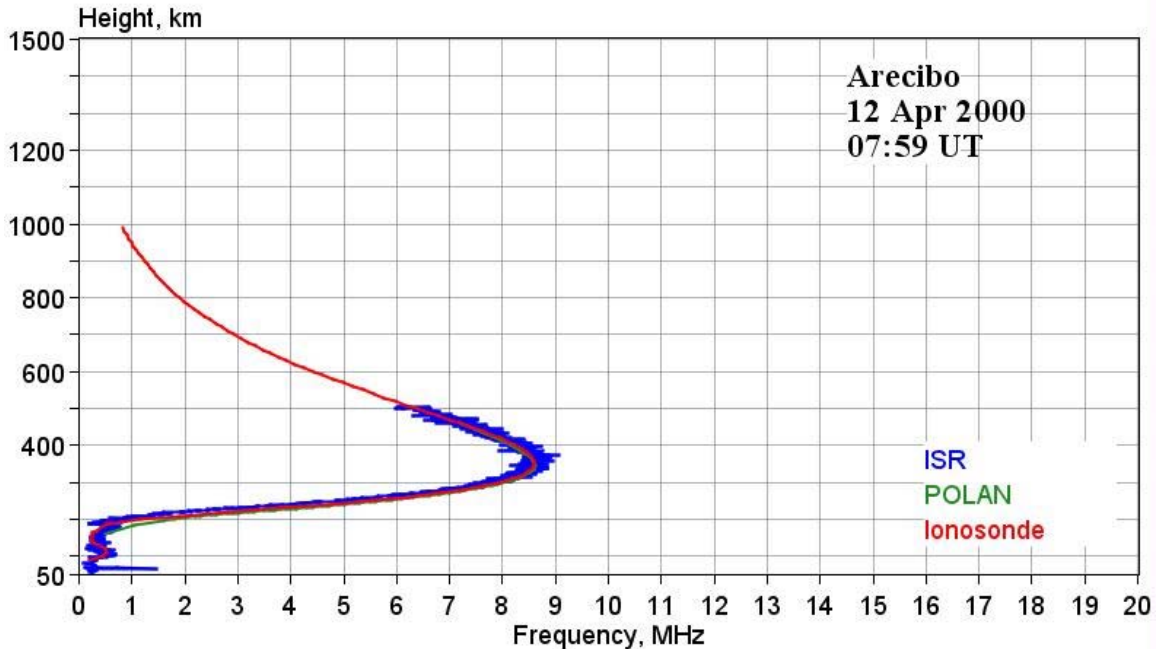


Figure 3. NHPC and POLAN profiles compared to radar data at Arecibo (high solar activity). NHPC (red curve) uses a night-time valley model, whereas POLAN uses a model for start height of ionosphere at 0.5 MHz.

Conducted study resulted in release of a new POLAN software version that corrects the night-time specification problem for use in the QualScan. Once the new POLAN was released, ARTIST-5 software was modified to include profile inversion uncertainty using a newly developed technique for calculation of per-point uncertainty from available profile boundaries that we described in our 2009 Annual Report. Newly calculated values are placed appropriately in the SAO.XML output files for deliveries to GAIM or other assimilative models.

### 3 HAARP INVESTIGATIONS

#### 3.1 Introduction

In our 2009 Annual Report, we had described the use of Gakona digisonde ionogram measurements to detect additional echo traces caused by the HAARP heating [Pedersen *et al.*, 2009] during the Fall 2008 HAARP Irregularities and Optics campaign, and the November 2009 campaign with two Digisonde 4D systems delivered and installed in Gakona and Tonsina. The new Digisonde 4D systems provided 10 sec cadence of the ionogram measurements that allowed unprecedented resolution of the artificial layer dynamics during the heating. During 2010, UMLCAR again participated in new joint multi-instrument HAARP campaigns dedicated to the study of the artificial density layers produced by the HF heating. This time the skymap capability of the originally installed DPS-4 digisonde model has been employed to detect and evaluate altitude profiles of the upflow plasma velocities.

### 3.2 February 2010 BRIOCHE Campaign

The February 2010 BRIOCHE heating campaign at HAARP was the first joint experiment involving *in situ* satellite and remote-sensing digisonde observations of ion outflows associated with artificial ducts produced by the HF heating. Data was provided by the DMSP satellites F15 and F16 overflying the heated region and by the Gakona digisonde running a dedicated high cadence skymap schedule. This was the first application of the skymap capability to the study of ionospheric HF heating. As a result, for the first time the artificial duct-related ion outflow was detected and evaluated in the bottom and topside F region simultaneously.

The Gakona/HAARP digisonde used its echo location capability to detect reflections of transmitted signals from irregular plasma structures in the ionosphere, placing the detected echoes on the skymap plane using their zenith and azimuth angles of arrival [Reinisch *et al.*, 1998]. Figure 4 presents two Doppler sky maps, one made just before the HF-heating the other made two minutes into the heating period. The measured Doppler shifts of the reflections are indicated by the color code. Negative Doppler shifts mean motion away from the sounder, i.e., upward motion for vertical or near vertical echoes. Figure 4 (top) shows that prior to heating the irregularities were evenly distributed with Doppler shifts close to zero, which indicates that there is little or no motion of the reflecting irregularities, neither vertical nor horizontal. Two minutes after the heater was turned on, a tight cluster of reflections appeared  $\pm 5^\circ$  about the magnetic zenith (MZ) (Figure 4, bottom). Note that the yellow color corresponds to negative Doppler shift, i.e., an average upward speed along the magnetic field line. Soon after the heater was turned off the strong “fast” echoes from the MZ disappeared.

Since the detected echoes come from the magnetic zenith, the measured line of sight velocity corresponds to the plasma motion along the magnetic field line. In earlier digisonde studies, Scali *et al.* [1995] had validated the digisonde line of site velocities by comparing collocated incoherent radar measurements with digisonde measurements at Sondrestrom, Greenland.

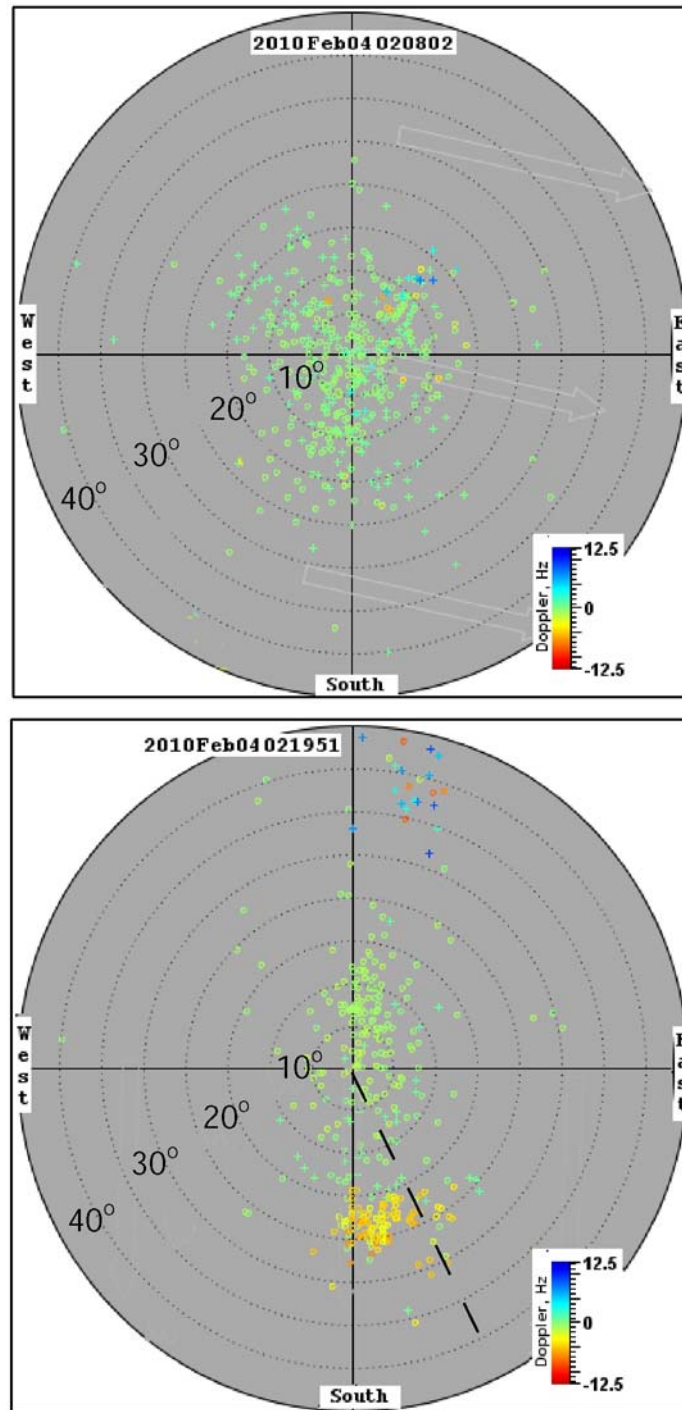


Figure 4. Doppler sky maps from the HAARP digisonde during the heating experiment 02/04/10: (top) 2 min prior and (bottom) 9 min into the HF-heating.

Figure 5 shows a waterfall display of the Doppler shift  $\Omega(r')$  measured for a given probing frequency  $f_p$  of 3,810 kHz at different virtual ranges  $r'$  between 335 and 370 km. As above, negative Doppler shifts correspond to the upward motion. Figure 5 reveals that the ion velocity increases with altitude. In fact, from Figure 5 one can obtain the upward ion velocity  $V_{up}^{\parallel}(r') = c(\Omega(r')/f_p)$  for different altitudes. Thus, we find that  $V_{up}^{\parallel}(335 \text{ km}) = 55 \pm 8 \text{ m/s}$ , while  $V_{up}^{\parallel}(370 \text{ km}) = 70 \pm 24 \text{ m/s}$ .

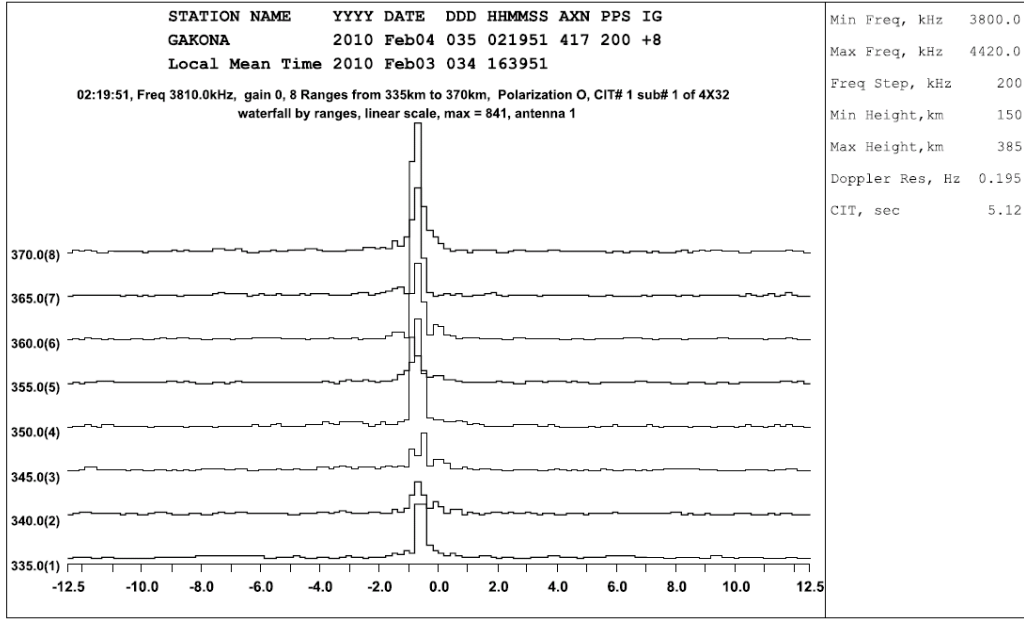


Figure 5. The Doppler shift for a given probing frequency measured at different altitudes between 335 and 370 km.

### 3.3 Progress in Analysis of November 2009 Campaign

During 2010, work continued on the analysis of the data collected during the November 2009 HAARP heating campaign. Along with the ionogram data collected, we began analyzing the data from the skymap measurements made by both digisonde systems at HAARP and Tonsina.

A comparison of the HF skymaps to the all-sky imager camera observations was made. Figure 6 shows simultaneous measurements made by the DPS-4D at HAARP and the collocated all-sky imager camera showing a very good agreement between the two techniques.

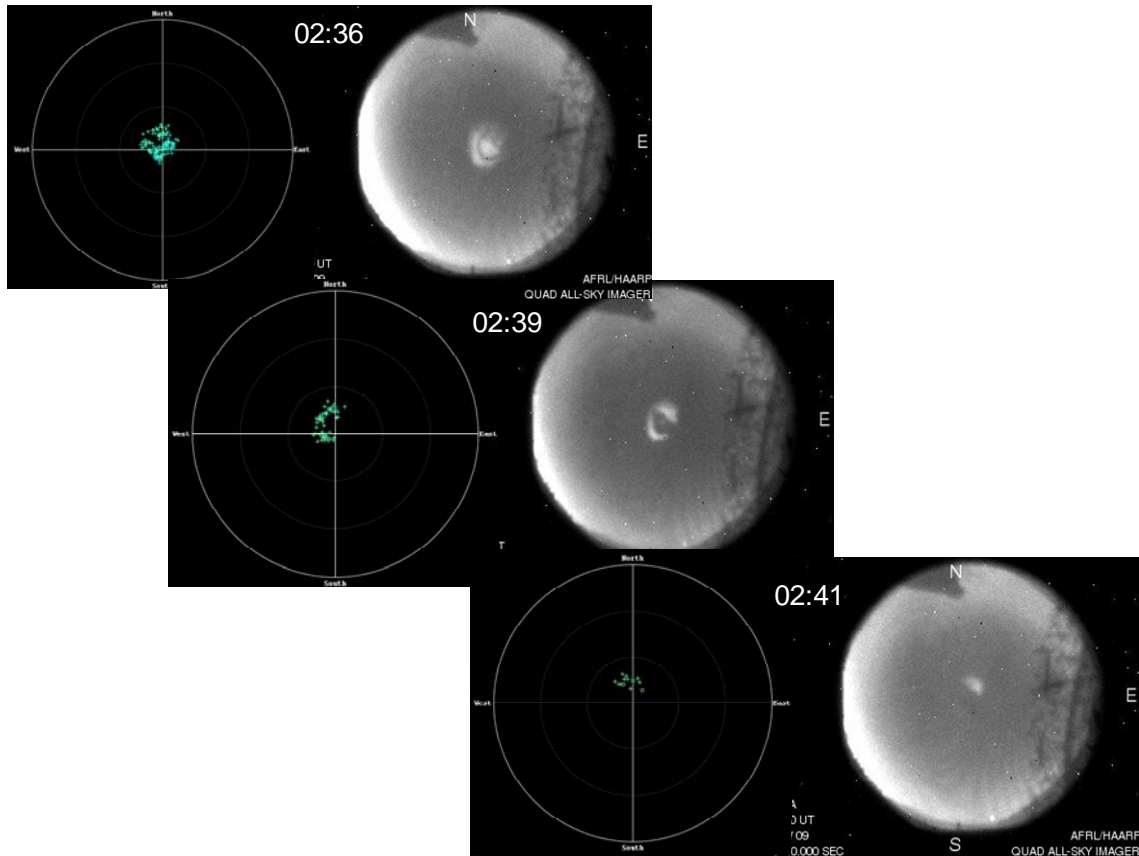


Figure 6. Simultaneous measurements made on November 16, 2009 by the HAARP DPS-4D system and the collocated all-sky camera. The skymap echoes in these maps come from the height of the additional layer observed in the ionogram. The HF and optical images are remarkably similar.

### 3.4 Upgrading the HAARP Digisonde Facility

Successful HAARP experiments involving the Digisonde 4D with its capability for 10-sec cadences of ionogram measurements and a high spatial resolution sensing of the altitude profiles of plasma motion have drawn attention to the new generation of the digisonde instrumentation and resulted in a decision to upgrade existing the Gakona DPS-4 model to the latest Digisonde 4D model. In preparation for the new 4D, custom software work has been initiated to optimize the operational capabilities of the new system in anticipation of the HAARP science modes, environment, operational practice, and new requirements for the data fidelity and system synchronization.

Table 1 presents a prioritized list of new Digisonde 4D software capabilities. Technical exchange between UMLCAR software sector and HAARP personnel responsible for digisonde operations has begun.

**Table 1. Prioritized Software Capabilities Guidance List**

#	Title	Description
1	Digisonde and HAARP Synchronization	The Digisonde and the HAARP transmitters shall be synchronized to enable HAARP to selectively turn off as the Digisonde passes through the HAARP frequency band that causes ionogram interference effects.
2	Pre-processed Data Archival	Preprocessed data archival to a large capacity external hard drive shall be remotely selectable. Preprocessed data formats shall be documented and provided to the government with unlimited rights.
3	Access to Real-time Data Acquisition	Multiple user access to real-time Digisonde data that impact timely Web access to Digisonde data. A capability to enable the same activities shall also be provided. acquisition shall be provided to assess ionospheric effects from and for frequency management of HAARP transmitter operations. The approach taken shall employ commercial off-the-shelf software that maximizes multiple user access and minimizes dropouts and slowdowns.
4	Data Processing Control	A remote, secure approach shall be provided to disable post processing and data communication activities

Software development in support of the upcoming upgrade of the HAARP sounder to Digisonde 4D model has been started. Time synchronization of the Digisonde 4D was reviewed and retested to conclude that measurement start is accurate to 5 ms. DCART software was enhanced to provide information screens detailing actual start UT of individual measurements within operational schedule to aid synchronous operations with the heater. Dispatcher software was reworked to separate data delivery activities into an independent thread so as to avoid processing tasks waiting for completion of the data delivery tasks. A technical meeting was held on November 22, 2010 to outline the roadmap for further software development during the next nine months.

### **3.5 Supporting HAARP experiments using the HAARP/Gakona Digisonde**

The UMLCAR team had received a number of requests to support various experiments conducted at HAARP by providing real time Digisonde data. For each of the experiments, a specific mode of the Digisonde operation appropriate for the science objective was set up. Table 2 lists the experiments for which UMLCAR provided digisonde support.

**Table 2. UMLCAR-supported experiments at HAARP**

PI	Experiment Title
M.C. Lee/J. Cohen	Generation of Large Plasma Sheets by HAARP Heater
V. Korotkikh	Generation of Ion outflow by HF-heating (DMSP)
S. Kuo	Simultaneous Generation of Large-Scale Density Irregularities and Geomagnetic Pulsations via Filamentation Instability
E. Mishin	In-situ detection of the plasma and neutral perturbations (CHAMP)
D. Papadopoulos	Generation of Ionospheric Ducts by HF-heating (DEMETER)
T. Pedersen	Production and detection of artificially enhanced density layers

### **3.6 Future Effort**

The initiated 4D software development will be completed.

## **4 RESEARCH INTO SELF-SCATTERING EFFECTS**

### **4.1 Introduction**

This research is a joint effort between the University of Massachusetts Lowell and the Institute of Radio Astronomy, Ukraine (IRA NASU) as described in our original BAA proposal. Previously, *Yampolski et al.* [2005] reported long-distance detection of transmissions from both EISCAT (Norway) and SURA (Russia) including observed motions of the irregularities generated by the heaters using the measured Doppler shifts of the received signals. These data were included into the original BAA proposal where it was suggested to extend those experiments by improving the detection and analysis of these effects with the use of an array of widely dispersed receivers.

The main objective of this research is to investigate the scattering of high power HF radio waves by ionospheric irregularities which are produced by the same HF emission (the “self-scattering effect”). In this study we used transmissions from the HAARP and EISCAT heaters to investigate this phenomenon. The HF radio waves self-scattered from the irregularities generated by the heater transmissions were monitored at several sites remote from the heater. In most locations a digisonde sounder was used as a receiver operating in a passive RF sensing mode. UMLCAR has developed a technique for using existing Digisondes in a narrow band mode to receive such signals.

### **4.2 February 2010 HAARP Scattering Campaign**

During this campaign, we ran test experiments at the HAARP heater on February 6 and 8, 2010. The objective was to test the operation of the heater in the special mode with two closely spaced frequencies, which may generate or enhance ion-acoustic waves. The tested frequency separations were 20, 40, and 60 Hz. The preliminary results suggest the possibility of self-

scattering effects in this mode at 2850 kHz, though results were not as clearly defined as in February 2008 when self-scattering was observed at 2755 kHz.

### **4.3 March 2010 EISCAT Campaign**

As planned, a special campaign with the EISCAT heater facility was carried out on 12-14 March, 2010. The operational mode was similar to the one tested at the HAARP heater in February 2010. As always, several dispersed receive sites were involved in this experiment, including the Ebro digisonde station.

During this short campaign, a very interesting effect was observed on one of the days. On March 14 at two stations, Kharkov (49.9° N, 36.9°E) and Irkutsk (52.8°N, 103.8°E), the scattered signals were observed simultaneously from 1330 UT to 1400 UT. The observed signals, however, had opposite Doppler shifts, and their intensities did not correlate with the changes in the HF heater power. We, therefore, stipulate that these particular signals were scattered on natural irregularities of electron density near the HF heater. It is known that at high-latitude and polar regions different types of irregularities exist, for example, “polar patches” (e.g., Weber *et al.*, 1984). During the experiment on March 14 such structures were indeed detected by the collocated Tromso Digisonde. Using the Doppler shifts recorded at the two sites, we were able to estimate the velocity (130 m/s) and direction of motion (almost exactly equatorward) of these structures.

## **5. D-REGION ABSORPTION USING DIGISONDE DATA**

### **5.1 Introduction**

Long distance radio communication is often limited by excessive D region absorption and real time drivers are required that can predict propagation outages. The measured amplitudes for vertical HF sounding are a reliable and sensitive measure of the D region absorption that can be made available from any digisonde station. Measurement of the absorption index will be one result of our research that can ultimately become part of a propagation forecast.

### **5.2 Median D-region profile**

To determine the diurnal variation of radio wave absorption using the echo amplitudes measured with an ionosonde, it is necessary to calibrate each sounder using nighttime data when there is no D-region contribution to the system losses. Following up on our previous work, using the digisonde data from Boulder, CO, the calibration was redone using a much expanded database for the same time period, i.e., May through August, 2005. The hours used in the analysis was expanded to 03 to 11 UT making it possible to calibrate over a larger frequency range, now reaching 6.9 MHz compared to 5.5 MHz, previously. Also, the frequency averaging was increased from five frequencies around the center frequency to seven frequencies. These time interval and frequency averaging changes significantly increased the size of the database used for the calibration.

The period from 10 August through 27 August 2005 was selected for noontime absorption analysis because that period was free from X-class flares but there occurred two M-class flares; one on 22 August and the other on 23 August during the daytime. Using the recently improved

system calibration technique developed earlier, the background median absorption for the hours around noontime ( $\pm 2$  hours) was calculated for the 17 days. The results are shown in Figure 7.

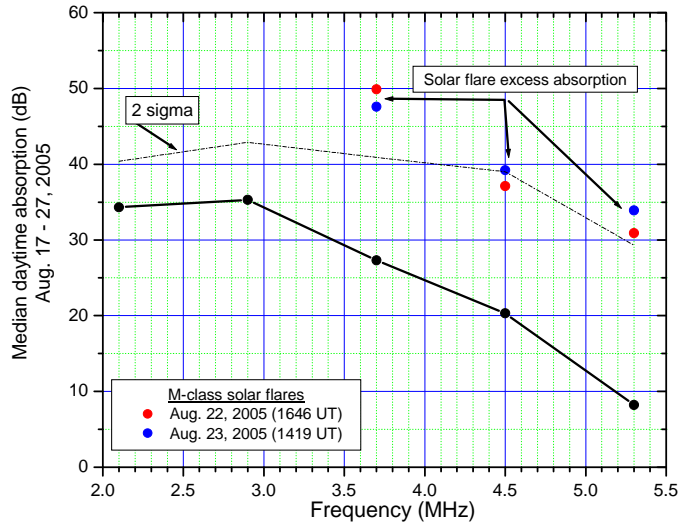


Figure 7. Median daytime absorption (dB) for Boulder, CO digisonde as a function of sounding frequency. Also shown is the upper 2-sigma curve for the routine measurements. The figure also shows the enhanced absorption following the two M-class flares on 22 and 23 August 2005.

The uncertainty in the absorption measurements is largest at 5.3 MHz. As discussed later, this impacts the electron density profile fitting process. On the average, the two flares produced approximately 20 dB excess absorption on frequencies between 3.2 and 5.3 MHz; no signal observations were available at the lower frequencies.

Using these absorption curves it was possible to derive a D-region electron density profile for the non-flare days and flare events. The first approach was to invert the absorption integral which is of the form of a Fredholm integral of the first kind. These integrals are notoriously difficult to solve and, unfortunately, we do not have the contractual resources to pursue this approach. The preliminary approach taken here was to derive the Ne-profile by using a trial and error method. Figure 8 shows the same absorption curve as Figure 7 as well as the absorption calculated using the derived electron density profile. Figure 9 shows the profile that was used to fit the digisonde median noontime absorption and the M-class flare absorption.

Four heights were used in the calculation of the Ne-profile to match the four sounding frequencies used in measuring the Digisonde absorption. For the median noontime measurements, the fit is exceedingly good except at the highest frequency (5.3 MHz). At this frequency the absorption has the greatest uncertainty. The question concerning the uniqueness of the derived Ne-profiles is certainly a subject for further investigation, but again limited resources prevented us from pursuing the issue any further at this time. These derived profiles (Figure 9)

shows what might be interpreted as a C-layer with a peak density of  $4.2 \times 10^8 \text{ m}^{-3}$  within the D-region.

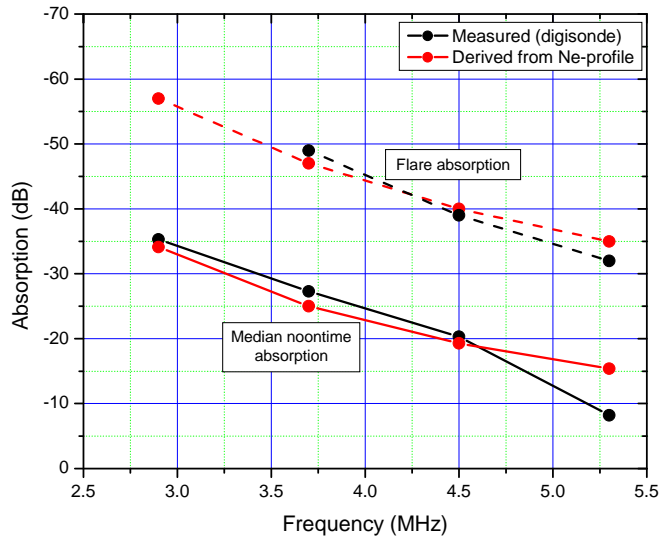


Figure 8. Absorption as a function of frequency for the August noontime data (solid curves). Black: digisonde absorption. Red: Absorption derived from the electron density profile. Flare absorptions are shown as dashed curves.

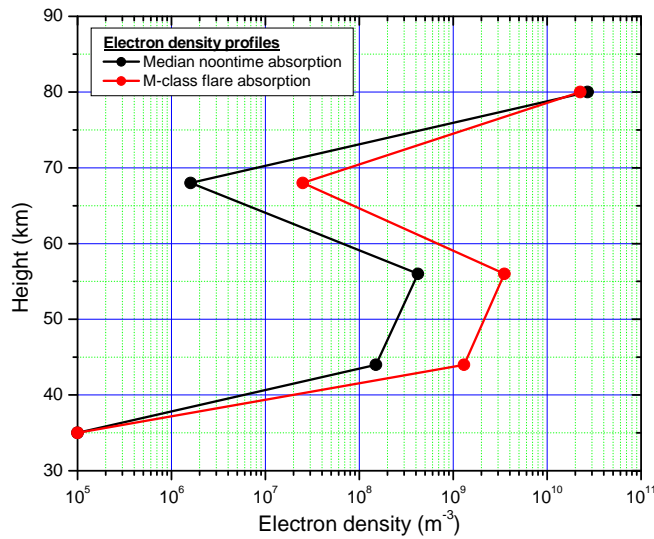


Figure 9. Derived electron density profiles that best fits the measured absorption data; black : median noontime profile. red : flare profile.

### 5.3 Flare profile

The same technique as used with the median noon data was used with the flare absorption data. The flare absorption is also depicted in Figure 7. The absorption at 2.9 MHz during the two flares was too great and no Digisonde echoes were detected. For this analysis, the absorption at 2.9 MHz was assumed to be 60 dB as compared to the next higher frequency at 3.7 MHz which was 49 dB, where a signal was detected. The flare absorption curve is presented in Figure 8 as the black dashed curve. The derived electron density profile that best fits these absorption data is shown in Figure 9. Between 45 km and 70 km there is approximately one order of magnitude increase in the electron density. This flare model fits the measured absorption very well as shown in Figure 8 (red-dashed curve). Ultimately, these models could be used to investigate D-region chemistry as well as the UV and X-ray components of the solar flare.

### 5.4 Recommendations

Using the new Digisonde 4D would make it possible to use the X-mode absorption rather than the O-mode that has always been used up to this point. The X-mode extends the effective frequency range; e.g., if the sounding frequency ranged from 2 to 5 MHz, O-mode (adding the electron cyclotron frequency), the effective frequency range would be from 3 to 6 MHz (assuming  $f_H = 1$  MHz) and the effective frequency ranges over a factor of 2. With the X-mode (subtracting  $f_H$ ) the effective frequencies would then be from 1 to 5 MHz, a frequency factor of 5.

## 6. STUDY OF THE IONOSPHERIC RESPONSE TO STRONG GEOMAGNETIC STORMS

### 6.1 Progress

The analysis of the ionospheric response to strong geomagnetic storms was extended to the low and equatorial latitude ionosphere. The approach and results obtained for the mid-latitude ionosphere have been described in detail in previous annual reports.

For this analysis, the following stations have been selected: Jicamarca (Geomagnetic Coordinates: 2.0 S, 355.3 E), Kwajalein (3.8 N, 238.2 E), Ascension Island (2.5 S, 56.8 E), and Ramey (28.6 N, 5.2 E). The strongest geomagnetic storms for recent years have been selected. These storms are listed in Table 1, where for each storm data availability and ionogram cadence are shown for each station together with the four quietest days selected for each storm in order to establish a quiet-day pattern.

All the ionograms available for the storm and quiet days listed in the table have been verified by human experts. The analysis has just begun. The ionospheric response to the geomagnetic disturbances will be analyzed using the peak characteristics of the F2 layer: foF2 and hmF2. Some interesting results have already been found. Figure 10 shows the data for the geomagnetic storm of 15 May 2005 recorded at Kwajalein. Interestingly, the effect of the geomagnetic disturbance on the layer height hmF2 is quite similar to that observed at middle latitudes (lower panel) with two strong upliftings observed soon after the storm commencement, but the effect on the electron density is much smaller (middle panel).

On other storm days, more interesting effects have been observed. Further analysis was based on our earlier work conducted for the middle-latitudinal ionosphere in the frame of this project [Paznukhov et al., 2009]. The main datasets used were ionogram records from digisonde stations stored in the University of Massachusetts Lowell Database (DIDBase). The following stations were used: Jicamarca (Geomagnetic Coordinates: 2.0 S, 355.3 E), Kwajalein (3.8 N, 238.2 E), Ascension Island (2.5 S, 56.8 E), Fortaleza (4.8 N, 33.7 W), and Ramey (28.6 N, 5.2 E). Thirty eight of the strongest geomagnetic storms from the recent years have been selected for analysis. All digisonde data have been manually processed (“scaled”) to assure the accuracy of

**Table 3. Major storms of 1997-2006**

Disturbed day	Quiet days	Jicamarca	Ascen.Is. (700 km)	Kwajalein	Ramey (700km)
10/10/1997	5 15 16 19 /10	30-min			
10/03/1998	7 8 9 18 /03	30-min			
18/10/1998	4 5 14 16 /10	30-min			
13/01/1999	3 19 26 30 /01	30-min			
18/02/1999	2 9 20 26 /02	1-hour			
22/09/1999	8 20 24 25 /09	30-min			
06/04/2000	14 18 22 25 /04	30-min	15-min		30-min
18/04/2001	19 24 25 27 /04		5-min		
21/10/2001	17 18 24 26 /10	1-hr			
28/10/2001	17 18 24 26 /10	1-hr			
06/11/2001	3 14 27 28 /11	15-min	5-min		
04/09/2002	20 23 24 25 /09	15-min			
07/09/2002	20 23 24 25 /09	15-min			
01/10/2002	23 24 25 29 /09	15-min			
29/05/2003	16 17 18 20 /05	15-min	15-min		
17/08/2003	4 5 16 27 /08	15-min	15-min		15-min
29/10/2003	10 11 12 23 /10	15-min	15-min		5,15-min
20/11/2003	8 27 28 29 /11	15-min	15-min		15-min
22/01/2004	12 14 29 31 /01	15-min	15-min		15-min
11/02/2004	8 10 17 20 /02	15-min	15-min		15-min
22/07/2004	7 8 9 21 /07	15-min	15-min		00-13UT
26/07/2004	7 8 9 21 /07	15-min	15-min		15-min
07/11/2004	2 5 6 15 /11	15-min	15-min	5-min	15-min
17/01/2005	9 25 26 27 /01	15-min	15-min		15-min
15/05/2005	5 24 25 26 /05	10-min	15-min	5-min	15-min
29/05/2005	5 24 25 26 /05	15-min		5-min	15-min
12/06/2005	10 20 27 28 /06	15-min	15-min	5-min	15-min
10/07/2005	5 6 8 24 /07	15-min	15-min	5-min	15-min
24/08/2005	11 12 20 28 /08	15-min	15-min	5-min	15-min
31/08/2005	11 12 20 28 /08	15-min	15-min	5-min	7-min
14/04/2006	1 2 3 12 /04	15-min	15-min	5-min	15-min

the measurements. The main electron density profile characteristics, hmF2 and foF2, were used in investigating the effects of the geomagnetic storms. In addition to the digisonde data used, large amounts of data characterizing the geomagnetic environment have been collected and analyzed (solar wind data, geomagnetic field variations, auroral activity indices). Our main findings and conclusions so far are as follows. 1) The major drivers for the ionospheric storm, electric field, and neutral wind have approximately equal importance at low- and equatorial latitudes. This is different from the middle latitude, where the neutral wind is a dominant factor. 2) The auroral index AE is the best precursor of the ionospheric effects at low- and equatorial latitudes. 3) Several very interesting cases of sudden very strong ionospheric uplifting suggest their possible relation to the equatorial super fountain effect. 4) During the famous super storm of 7-8 November 2004 [e.g., Maruyama, 2006] the penetration electric field alone is not capable of producing the ionospheric effects on a global scale.

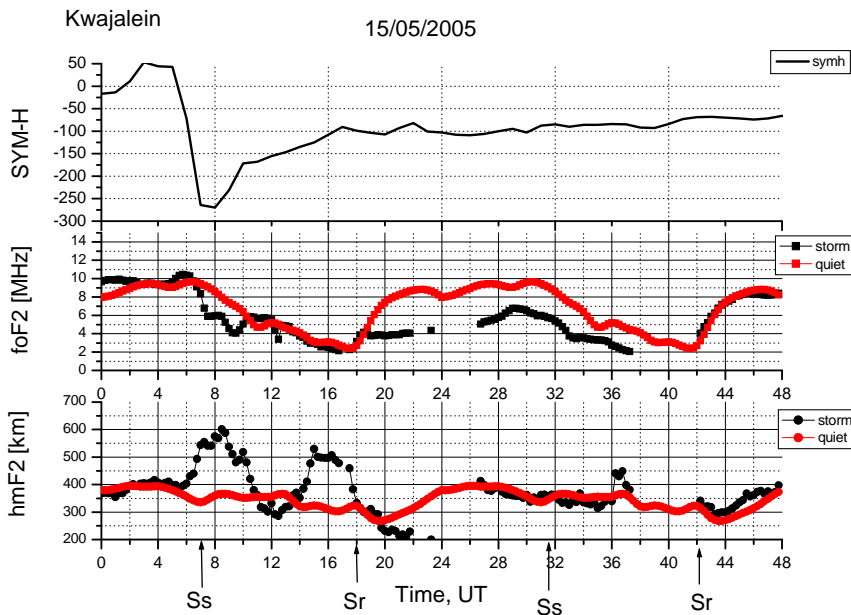


Figure 1. Geomagnetic storm of 15 May 2005 as observed with the DPS-4 at Kwajalein. The effect on the ionospheric layer height is clearly seen (lower panel). The effect on the electron density (middle panel) is significantly weaker.

## 7 COMPARING COSMIC/FORMOSAT EDP WITH DIGISONDE PROFILES

### 7.1 Introduction

We worked on the analysis of the accuracy of COSMIC Radio Occultation (RO) measurements as a function of occultation geometry, namely the length of the projection of the occultation tangent points (for which EDP is calculated), conventionally referred to as *horizontal smear*. Figure 11 shows an example of RO measurements made in the vicinity of Kwajalein on February 17, 2007 and visualizes the smear parameter. While horizontal smears greatly vary for different occultations, for the purpose of the comparison, only measurements with smears smaller than 2000 km were selected.

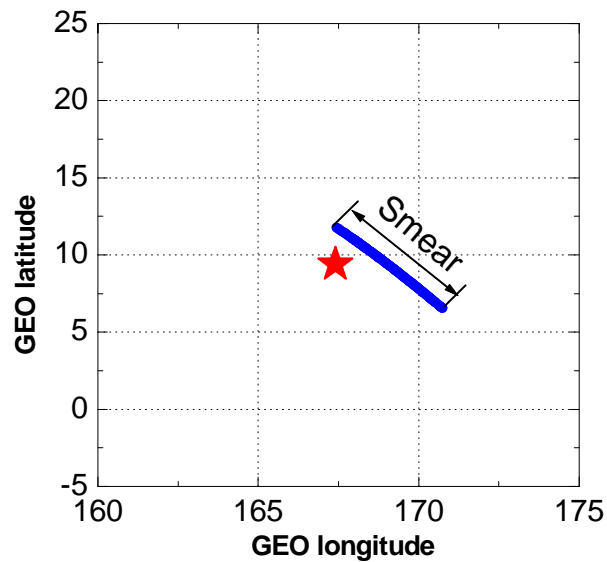


Figure 11. RO measurement made in the vicinity of Kwajalein station on February 17, 2007. The blue symbols show radial projections of tangent points at which electron density is measured. The red star indicates the Kwajalein digisonde location. Horizontal smear parameter represents the length of the projection.

In the RO technique, the vertical EDP is calculated under the assumption of local spherical symmetry of the electron density distribution in the region where the measurement is made. The size of the region is defined by a horizontal smear of a particular occultation. We analyzed the dependence of the RO electron density measurements errors on the horizontal smear of the occultations. It is expected that larger errors are associated with larger smears, since any existing horizontal gradients more significantly violate the assumption of spherical symmetry in the electron density distribution.

The data processing algorithm to study the effect of the occultation smear is rather straightforward: RO measurement error is calculated as a function of the occultation smear.

Figure 12 shows absolute values of the difference between the electron densities simultaneously determined with the RO and digisonde techniques for the same heights for Tromso in the period from December 2006 to May 2007. Over one thousand individual data points are shown.

We made the same type of analysis for three stations, Tromso, Kwajalein, and Ebro, Spain. Figures 13, 14, and 15 present RO electron density measurement errors versus smear lengths.

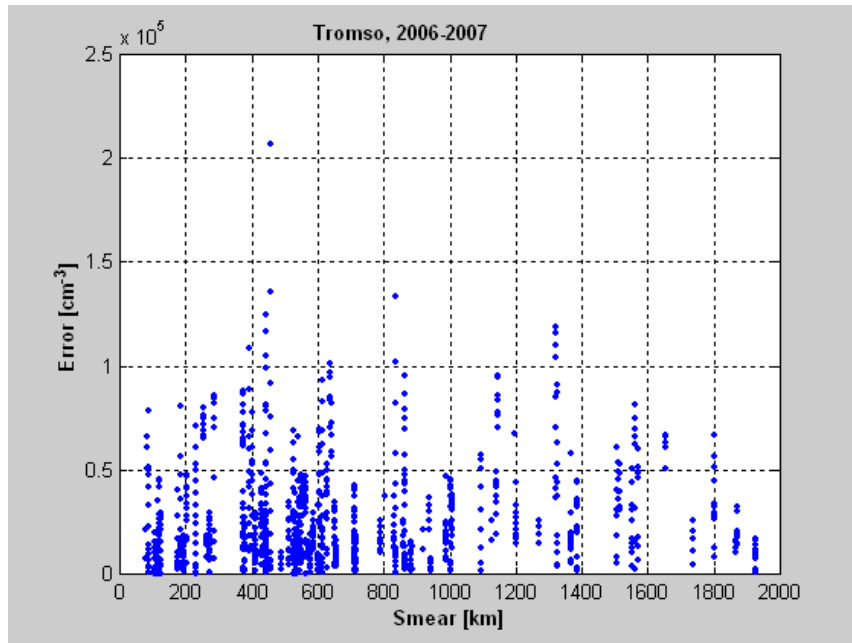


Figure 12. RO measurement error as a function of occultation smear calculated for Tromso location. Majority of measurements have horizontal smears smaller than 1000 km.

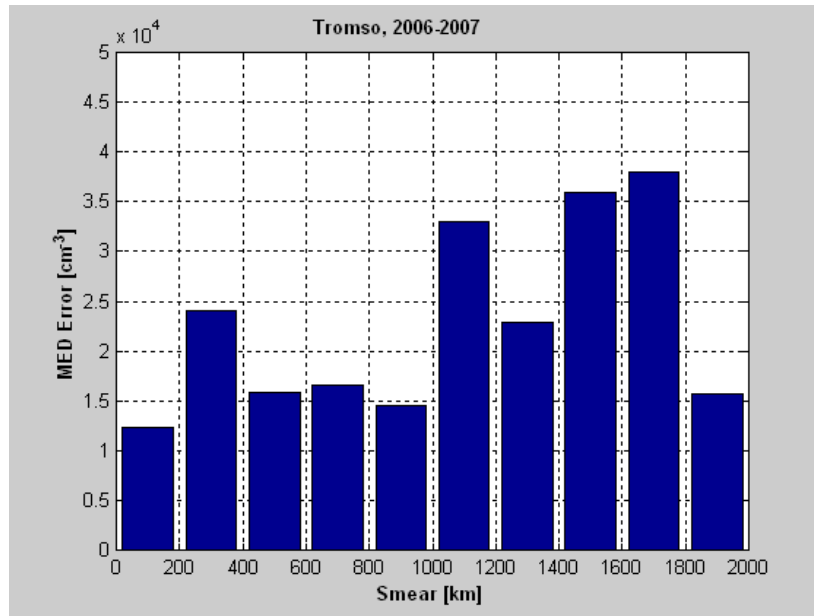


Figure 13. RO measurement error as a function of occultation smear calculated for Tromso. The data are binned according to the smear value, and the median error is calculated for each data bin. The overall trend indicates larger errors for greater horizontal smears.

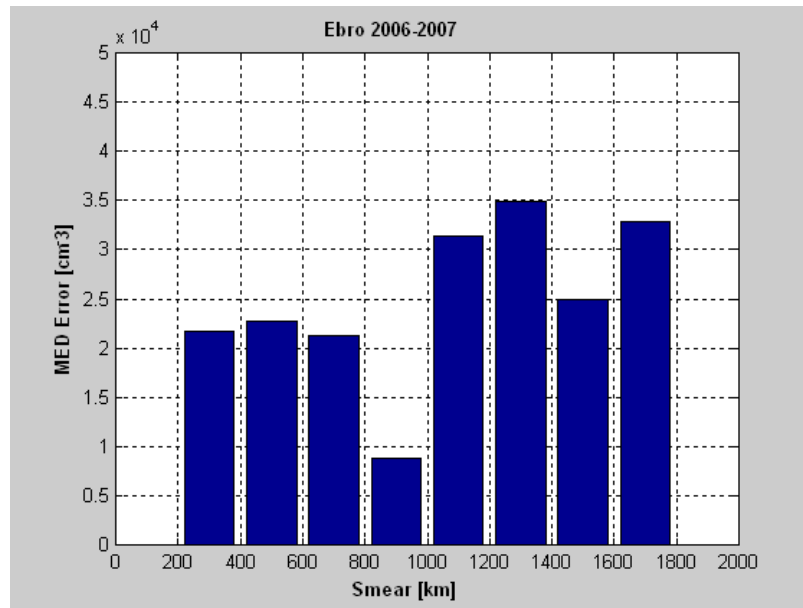


Figure 14. RO measurement error as a function of occultation smear calculated for Ebro. The data are binned according to the smear value, and median error is calculated for each data bin. The overall trend shows larger error for greater horizontal smears, as expected.

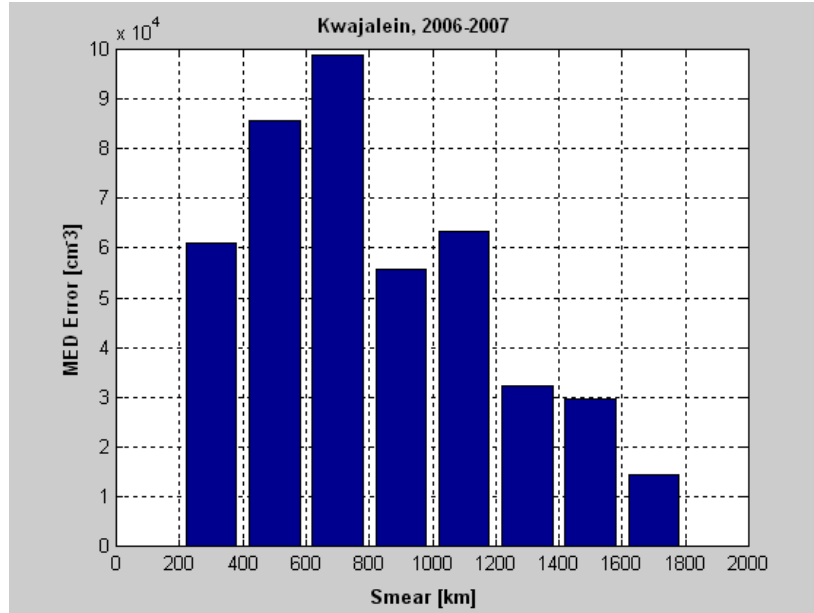


Figure 15. RO measurement error as a function of occultation smear calculated for Kwajalein. Note different scale of the y-axis with respect to Figure 11. The data are binned according to the smear value, and median error is calculated for each data bin.

For the Ebro data, shown in Figure 14, there is a general trend toward larger errors for increasing smear values. This result is in agreement with that obtained for Tromso (Figure 13) and agrees with our a priori expectation. Kwajalein data, however, showed an unexpected trend, with the maximum error corresponding to the horizontal smears between 500-700 kilometers. For larger smears the error in RO measurements turns out to be smaller. Therefore, it can be concluded that for the equatorial region the horizontal smear is not a major factor determining the accuracy of RO measurements. This result is surprising and so far not understood.

## PUBLICATIONS

The following journal publications have acknowledged support under AFRL Contract No. FA8718-06-C-0072.

Aragon-Angel, A., Y.-A. Liou, C.-C. Lee, B.W. Reinisch, M. Hernández-Pajares, M. Juan, J. Sanz, Improvement of retrieved FORMOSAT-3/COSMIC electron densities validated by using Jicamarca DPS measurements, submitted, *Radio Sci.*, 2010.

Krause, H., L., P. Straus, and B. W. Reinisch, Ionospheric plasma density profiles: A comparison between C/NOFS occultation receiver for ionospheric sensing and specification (CORISS) and digisonde observations, *Radio Sci.*, submitted, 2010.

Milikh, G. M. E. Mishin, I. Galkin, A. Vartanyan, C. Roth, and B. W. Reinisch, Ion outflows and artificial ducts in the topside ionosphere at HAARP, *Geophys. Res. Lett.*, 37, L18102, doi:10.1029/2010GL044636, 2010

Pedersen, T., M. McCarrick, B. Reinisch, B. Watkins, R. Hamel, and V. Paznukhov, Production of artificial ionospheric layers by frequency sweeping near the 2<sup>nd</sup> gyroharmonic, submitted, *Geophys. Res. Lett.*, 2010.

Reinisch, Bodo W. and Ivan A. Galkin, Global ionospheric radio observatory (GIRO), accepted, *Earth, Planets, and Space*, 2010.

Zhao, Biqiang, Weixing Wan, Bodo Reinisch, Xinan Yue, Huijun Le, Jing Liu, and Bo Xiong, Features of the F3 layer in the low-latitude ionosphere at sunset, submitted, *J. Geophys. Res.*, 2010.

Zong, Q.-G., B. W. Reinisch, P. Song, Y. Wei, and I. Galkin, Dayside ionospheric response to the intense interplanetary shocks/solar wind discontinuities: Observations from the digisonde global ionospheric radio observatory, *J. Geophys. Res.*, 115, A06304, doi:10.1029/2009JA014796, 2010.

Abdu, M. A., I. S. Batista, B. W. Reinisch, J. R. de Souza, J. H. A. Sobral, T. R. Pedersen, A. F. Medeiros, N. J. Schuch, E. R. de Paula, and K. M. Groves, Conjugate point equatorial experiment (COPEX) campaign in **Brazil** : Electrodynamics highlights on spread F development conditions and day-to-day variability, *J. Geophys. Res.*, 114, A04308, doi:10.1029/2008JA013749, 2009.

Ayub, M., S. Iqbal, M. A. Ameen, and B. W. Reinisch, Study of maximum electron density  $N_mF_2$  at Karachi and Islamabad during solar minimum (1996) and solar maximum (2000) and its comparison with IRI, *Adv. Space Res.*, 43, 11, 1821-1824, 2009.

Kutiev, I, P. Marinov, A. Belehaki, B. Reinisch and N. Jakowski, Reconstruction of topside density profile by using the topside sounder model profiler and digisonde data, *Adv. Space Res.*, 43, 1683–1687, 2009.

Lin, C. H., A. D. Richmond, J. Y. Liu, G. J. Bailey, and B. W. Reinisch, Theoretical study of new plasma structures in the low-latitude ionosphere during a major magnetic storm, *J. Geophys. Res.*, *114*, A05303, doi:10.1029/2008JA013951, 2009.

Paznukhov, V. V., D. Altadill, and B. W. Reinisch, **Experimental evidence for the role of the neutral wind in the development of ionospheric storms in mid-latitudes**, *J. Geophys. Res.*, **114**, A12319, doi:10.1029/2009JA014479, 2009.

Ram, S. Tulasi S.-Y. Su, C. H. Liu, B. W. Reinisch, and Lee-Anne McKinnell, Topside ionospheric effective scale heights (HT) derived with ROCSAT-1 and ground-based ionosonde observations at equatorial and mid-latitude stations, *J. Geophys. Res.*, *114*, A10309, doi:10.1029/2009JA014485, 2009.

Reinisch, B. W., I. A. Galkin, G. M. Khmyrov, A. V. Kozlov, K. Bibl, I. A. Lisysyan, G. P. Cheney, X. Huang, D. F. Kitrosser, V.V. Paznukhov, Y. Luo, W. Jones, S. Stelmash, R. Hamel, and J. Grochmal, The New Digisonde for Research and Monitoring Applications, *Radio Sci.*, *44*, RS0A24, doi:10.1029/2008RS004115, 2009.



## REFERENCES

- Chen, C.F., B.W. Reinisch, J. L. Scali, X. Huang, R. R. Gamache, M. J. Buonsanto and B.D. Ward, The accuracy of ionogram-derived N(h) profiles, *Adv. Space Res.*, 14, 12, 43-46, 1994.
- Huang, X. and B. W. Reinisch, Automatic calculation of electron density profiles from digital ionograms. 2. True height inversion of topside ionograms with the profile-fitting method, *Radio Sci.*, 17, 837-844, 1982.
- Huang, X. and B. W. Reinisch, Vertical electron density profiles from the digisonde network, *Adv. Space Res.*, 18, 121-129, 1996.
- Huang, X. and B. W. Reinisch, Real time HF raytracing through a tilted ionosphere, *Radio Sci.*, 41(5), RS5S47, 10.1029/2005RS003378, 2006.
- McNamara, Leo F., Craig R. Baker, Dwight T Decker, Accuracy of USU-GAIM specifications of foF2 and M(3000)F2 for a worldwide distribution of ionosonde locations, *Radio Sci.*, 43, 1, RS1011 10.1029/2007RS003754, 2008.
- McNamara, Leo F., Quality figures and error bars for autoscaled Digisonde vertical incidence ionograms, *Radio Sci.*, 41, RS4011, doi:10.1029/2005RS003440, 2006.
- Paznukhov, V. V., D. Altadill, and B. W. Reinisch, Experimental evidence for the role of the neutral wind in the development of ionospheric storms in midlatitudes, *J. Geophys. Res.*, 114, A12319, doi:10.1029/2009JA014479, 2009.
- Pedersen, T., B. Gustavsson, E. Mishin, E. MacKenzie, H. C. Carlson, M. Starks, T. Mills, Optical ring formation and ionization production in high-power HF heating experiments at HAARP, *Geophys. Res. Lett.*, 36, L18107, 4, doi:10.1029/2009GL040047, 2009,
- Reinisch, B. W., R. R. Gamache, X. Huang, and L. F. McNamara, Real time electron density profiles from ionograms, *Adv. Space Res.*, 8, 63-72, 1988.
- Reinisch, Bodo W. and Ivan A. Galkin, Global ionospheric radio observatory (GIRO), accepted, *Earth, Planets, and Space*, 2010.
- Reinisch, B. W., I. A. Galkin, G. Khmyrov, A. Kozlov, and D. F. Kitrosser, Automated collection and dissemination of ionospheric data from the digisonde network, *Adv. Radio Sci.*, 2, 241-247, 2004.
- Titheridge, J. E., Ionogram analysis: Least squares fitting of a Chapman peak, *Radio Sci.*, 20(2), 247-256, 1985.
- Titheridge, J. E. (1988), The real height analysis of ionograms: A generalized formulation, *Radio Sci.*, 23(5), 831-849, doi:10.1029/RS023i005p00831.

Weber, E. J., J. Buchau, J. G. Moore, J. R. Sharber, R. C. Livingston, J. D. Winningham, and B. W. Reinisch, F-layer ionization patches in the polar cap, *J. Geophys. Res.*, 89, 16832-1694, 1984.